


# Thermally-enhanced charge collection boosts photoelectrochemical performance of hematite

Yujie Wang(王玉杰), Xu Cheng(程旭), Jialin Shao(邵嘉琳), Xugang Qi(漆旭刚), Jia Zhao(赵嘉), Lu Yang(杨露), Youwei Zhang(张有为), Bonan Zhu(朱博南), and Zemin Zhang(张泽民)

**Citation:**Chin. Phys. B, 2026, 35 (**5**): 058201. DOI: 10.1088/1674-1056/ae37fc
http://cpb.iphy.ac.cn; http://iopscience.iop.org/cpb

**What follows is a list of articles you may be interested in**

---

## Screening *A*-site ordered quadruple perovskites for alkaline hydrogen evolution reaction via unifying electronic configuration descriptor

Ning Sun(孙宁), Wenbo Li(李文博), Yang Qin(秦杨), Zhichuan Zheng(郑智钏), Bowen Zhang(张博文), Xiangjiang Dong(董祥江), Peng Wei(魏鹏), Yixiao Zhang(张艺潇), Xian He(何贤), Xinyu Xie(谢新煜), Kai Huang(黄凯), Lailei Wu(吴来磊), Ming Lei(雷鸣), Huiyang Gou(缑慧阳), and Runze Yu(于润泽)
Chin. Phys. B, 2024, 33 (**12**): 128101. DOI: 10.1088/1674-1056/ad8074

## Experimental investigation of omnidirectional multiphysics bilayer invisibility cloak with anisotropic geometry

Huolei Feng(丰火雷), Xingwei Zhang(张兴伟), Limin Zhou(周利敏), Yuekai Zhang(张悦凯), and Yushan Ni(倪玉山)
Chin. Phys. B, 2024, 33 (**3**): 038102. DOI: 10.1088/1674-1056/acf490

## MatChat: A large language model and application service platform for materials science

Zi-Yi Chen(陈子逸), Fan-Kai Xie(谢帆恺), Meng Wan(万萌), Yang Yuan(袁扬), Miao Liu(刘淼), Zong-Guo Wang(王宗国), Sheng Meng(孟胜), and Yan-Gang Wang(王彦棡)
Chin. Phys. B, 2023, 32 (**11**): 118104. DOI: 10.1088/1674-1056/ad04cb

## Tuning the particle size, physical properties, and photocatalytic activity of $Ag_3PO_4$ materials by changing the $Ag^+/PO_4^{3-}$ ratio

Hung N M, Oanh L T M, Chung D P, Thang D V, Mai V T, Hang L T, and Minh N V
Chin. Phys. B, 2023, 32 (**3**): 038102. DOI: 10.1088/1674-1056/ac84ce

## Hydrodynamic metamaterials for flow manipulation: Functions and prospects

Bin Wang(王斌) and Jiping Huang (黄吉平)
Chin. Phys. B, 2022, 31 (**9**): 098101. DOI: 10.1088/1674-1056/ac7f8c

---

**RAPID COMMUNICATION**

# Thermally-enhanced charge collection boosts photoelectrochemical performance of hematite

Yujie Wang(王玉杰)[1,†], Xu Cheng(程旭)[2,†], Jialin Shao(邵嘉琳)[1], Xugang Qi(漆旭刚)[1], Jia Zhao(赵嘉)[1], Lu Yang(杨露)[1], Youwei Zhang(张有为)[3,‡], Bonan Zhu(朱博南)[2,§], and Zemin Zhang(张泽民)[1,¶]

[1] *School of Physical Science and Technology, Key Laboratory of Special Functional Materials and Devices, Ministry of Education, Lanzhou University, Lanzhou* 730000, *China*

[2] *School of Aerospace Engineering, Beijing Institute of Technology, Beijing* 100081, *China*

[3] *School of Physics, Huazhong University of Science and Technology, Wuhan* 430074, *China*

(Received 2 December 2025; revised manuscript received 8 January 2026; accepted manuscript online 14 January 2026)

The application of transition metal oxides in optoelectronics holds significant promise. However, their performance is often limited by small polaron hopping, a charge transport mechanism that reduces carrier mobility and collection efficiency. Therefore, improving small polaron hopping is crucial for enhancing charge collection. In this work, we propose a direct approach to effectively enhance the photoelectrochemical (PEC) performance of hematite by leveraging the thermal nature of polaron hopping. As a result, a photocurrent density of 4.53 mA/cm$^2$ at 1.23 V vs. RHE was achieved by heating the photoanode to 70 °C. By combining carrier dynamics analysis with charge collection modeling, we demonstrate that heating facilitates small polaron hopping, thereby increasing carrier mobility and improving the collection efficiency of hematite photoanodes. Our work provides clear explanations of the thermal-activated small polaron hopping mechanism, offering a simple yet effective strategy for enhancing the PEC performance of transition metal oxides.

**Keywords:** small polaron hopping, hematite, thermal activation, transfer matrix model

**PACS:** 82.80.Fk, 81.05.Zx, 84.60.Jt, 64.70.ph

**DOI:** 10.1088/1674-1056/ae37fc **CSTR:** 32038.14.CPB.ae37fc

## 1. Introduction

Photoelectrochemical (PEC) technology offers a promising route for converting solar energy directly into chemical fuels.[1,2] In a PEC device, a semiconductor photoelectrode absorbs light to generate charge carriers, which then separate and migrate to the surface to drive redox reactions.[3] Hematite ($\alpha$-$Fe_2O_3$) is a particularly attractive photoanode material for this purpose due to its earth-abundant, chemical stability, and ideal band gap (2.1 eV) for visible light absorption.[4–7] However, despite these advantages, the practical application of hematite is severely limited by its intrinsically poor carrier transport properties, which lead to high rates of electron–hole recombination and consequently low energy conversion efficiency (Fig. 1(a)).[7–10]

The root of this poor performance lies in the formation of small polarons, a process greatly facilitated by intrinsic defects within the material.[8,10,11] Under photoexcitation, electrons in $\alpha$-$Fe_2O_3$ will hop from O 2p orbitals to Fe 3d orbitals (Fig. 1($b_i$)).[4] Instead of moving freely through the crystal lattice, photoexcited electrons localize on iron atoms, creating a localized lattice distortion, known as a small polaron. This intense localization creates a strong electrostatic interaction that physically distorts the surrounding lattice.[4,12] Charge transport then occurs via a slow, thermally-activated "hopping" of these polarons between lattice sites, rather than through fast band-like conduction (Fig. 1($b_{ii}$)).[13–15] Oxygen vacancies ($O_V$) are intrinsic defects in $\alpha$-$Fe_2O_3$, and act as trapping sites that further localize polarons and exacerbate recombination.[16,17]

To address this critical transport limitation, research has primarily focused on strategies like elemental doping and surface passivation. Doping can modify the electronic environment to lower the energy barrier for polaron hopping, while surface passivation aims to reduce the density of surface defects (including $O_V$).[18–20] While effective to some extent, these methods often involve complex, multi-step fabrication processes that may introduce impurities or create secondary issues. We propose a more direct approach: leveraging the thermal nature of polaron hopping.[10,14,21,22] Since hopping is a thermally-activated process, raising the temperature can increase the hopping frequency and liberate polarons from trapping sites, effectively increasing charge carrier mobility (Fig. 1($b_{iii}$)).[10,11,21,23]

[†]These authors contributed equally to this work.

[‡]Corresponding author. E-mail: youweizhang@hust.edu.cn

[§]Corresponding author. E-mail: bzhu@bit.edu.cn

[¶]Corresponding author. E-mail: zhangzemin@lzu.edu.cn

© 2026 Chinese Physical Society and IOP Publishing Ltd. All rights, including for text and data mining, AI training, and similar technologies, are reserved.

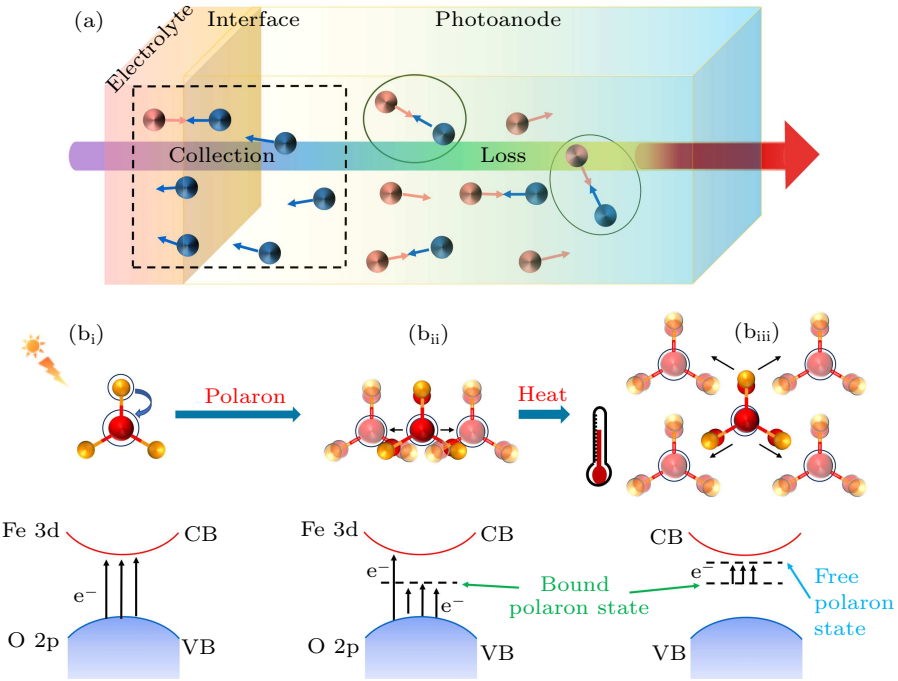



**Fig. 1.** Mechanism of the effect of small polaron hopping on carrier transport. (a) Schematic of carrier transport from the photoanode to the electrolyte–photoanode interface after photoexcitation. (b) Diagrams illustrating the formation of small polarons and the enhancement of their activity along with the corresponding energy band plots.

In this work, we thoroughly investigated the thermally-regulated dynamics of small polarons in $\alpha$-$Fe_2O_3$ combining computational and experimental approaches. Annealing $\alpha$-$Fe_2O_3$ samples in an argon atmosphere increases the concentration of $O_V$, giving rise to defect states within the band gap as indicated by density functional theory (DFT) calculations. This increases the probability of small polaron formation, facilitating our study of small polarons within the samples. Calculations of carrier separation and injection efficiency, as well as mobility tests, demonstrate that temperature elevation promotes small polaron hopping and increases the carrier mobility, which is the primary reason for the enhanced PEC performance. Ultimately, analysis of the spatial loss rate (SLR) suggests that elevated temperature enhances the carrier collection efficiency. Our work provides a practical and effective approach for enhancing the water-splitting performance of small polaron dominated transition metal oxides.

## 2. Results and discussion

### 2.1. Material characterization

Figure 2(a) depicts a cross-section scanning electron microscope (SEM) of $\alpha$-$Fe_2O_3$, with an approximate thickness of 200 nm. The plane-view SEM and energy dispersive spectrometer (EDS) are available in Figs. S1 and S2.[24] X-ray diffraction (XRD) was performed on the film after being annealed at 700 °C in an argon atmosphere on an FTO substrate. The resulting pattern demonstrates that the $\alpha$-$Fe_2O_3$ is well-oriented on the (110) crystal plane (Fig. 2(d)).[25] XRD patterns of other treated hematite samples are presented in Fig. S3. To probe the effect of the annealing atmosphere, x-ray photoelectron spectroscopy (XPS) was used. The spectra for the O 1s orbitals (Figs. 2(b) and 2(c)) indicate that the argon annealing process yields a higher concentration of $O_V$ compared to annealing in air.[8,26,27] DFT calculations were performed to understand the electronic impact of these vacancies. The calculated density of states (DOS) and energy band structures (Fig. S4) show that introducing $O_V$ creates a new defect state at the bottom of the conduction band (Fig. 2(f)), which is absent in the defect-free $\alpha$-$Fe_2O_3$ (Fig. 2(e)). Such a defect state, positioned within the band gap or slightly below the CBM, serves as an electron trapping site, leading to significant charge localization and concomitant local lattice distortions, key hallmarks of small polaron formation.[15,28] This phenomenon is critical for understanding charge transport and photocatalytic activity in $\alpha$-$Fe_2O_3$. Therefore, to study this phenomenon in depth, the argon-treated $\alpha$-$Fe_2O_3$ samples with higher vacancy concentration were selected for all subsequent experiments.

Figure 2(g) illustrates *in-situ* Raman spectra of the $\alpha$-$Fe_2O_3$, recorded using 633 nm optical excitation at temperatures ranging from room temperature down to −180 °C. It can be observed that the intensity of each peak decreases in proportion to the increase in temperature, and the Raman peaks are red-shifted.[29,30] This is because higher temperatures enhance phonon–phonon interactions and anharmonic electron–phonon coupling.[30–32] These intensified interactions weaken the strong coupling between electrons and specific phonon modes, thereby reducing the localization of small polarons. This, in turn, strengthens lattice vibrations, causing the red

shift of the Raman peaks.[30–32] Simultaneously, the lattice undergoes thermal expansion, leading to a shallower depth of the localized lattice distortion potential well and lowering the energy barrier for confining small polarons. Meanwhile, the lattice thermal expansion also weakens thermal conductivity and reduces the Raman peak intensity.[30,32] These synergistic effects collectively lower the activation energy required for small polarons hopping, enhancing the charge transport capabilities. The Raman spectrum taken at room temperature with 532 nm photoexcitation is provided in Fig. S5.

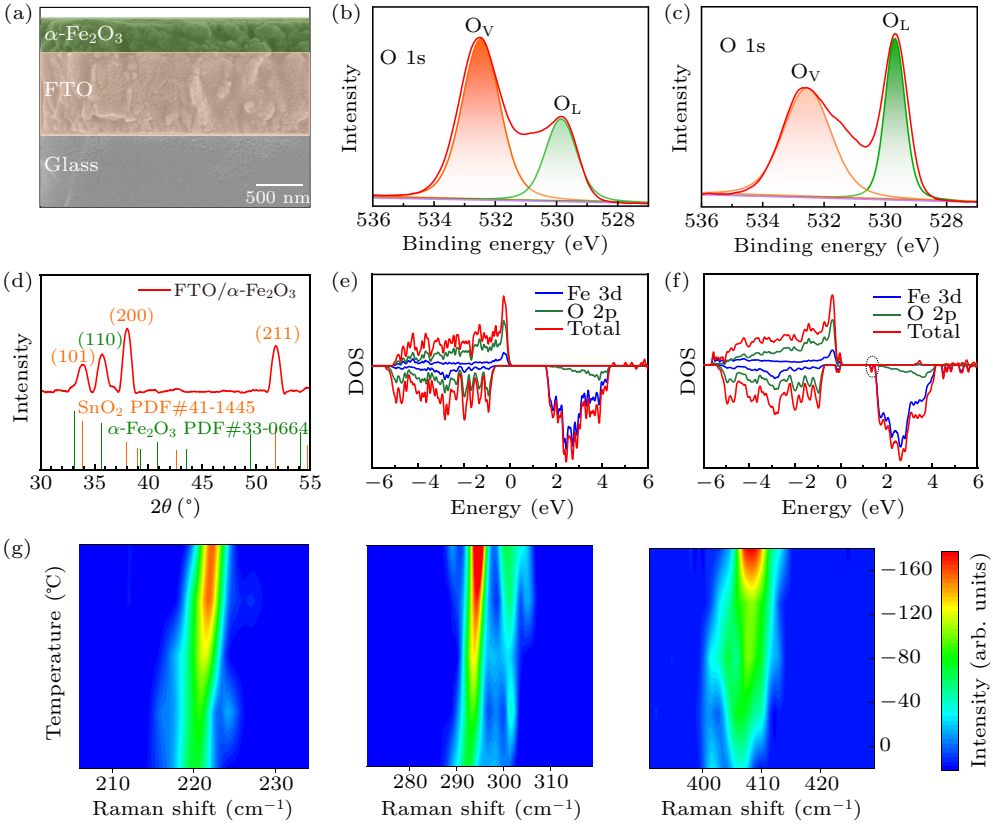



**Fig. 2.** Material characterization. (a) Cross-section SEM of $\alpha$-$Fe_2O_3$ film; XPS image of O 1s orbitals of $\alpha$-$Fe_2O_3$ treated in (b) argon and (c) air; (d) XRD spectrum of $\alpha$-$Fe_2O_3$ annealed in argon at 700 °C; DOS of $\alpha$-$Fe_2O_3$ (f) with and (e) without additional $O_V$. (g) Variable temperature Raman spectra of $\alpha$-$Fe_2O_3$ in different wavelength ranges.

### 2.2. Thermally-regulated PEC performance

The PEC characteristics of the argon-treated $\alpha$-$Fe_2O_3$ photoelectrodes were investigated, focusing on the effects of operating temperature. Linear scan voltammetry (LSV) under simulated AM 1.5G solar illumination shows that heating the system significantly boosts performance (Fig. 3(a)). Figure S6 shows that introducing $O_V$ results in a greater increase in performance after heating. At a potential of 1.23 V vs. RHE, the net photocurrent density increased by a factor of 1.69, rising from 2.68 mA/cm$^2$ at 25 °C to 4.53 mA/cm$^2$ at 70 °C. This enhancement is supported by incident photon-to-current conversion efficiency (IPCE) measurements (Fig. 3(b)), which show a 1.6-fold increase at a wavelength of 360 nm at 70 °C compared to room temperature. These results clearly demonstrate that heating is a simple and effective technique for improving the photoelectrode's performance.

To determine the cause of this improvement, the physical properties of the $\alpha$-$Fe_2O_3$ film were analyzed. The light absorption increased only marginally upon heating and is thus an unlikely contributor to the large performance gain (Fig. S7). Similarly, Mott–Schottky analysis (Fig. 3(c)) revealed that the carrier concentration rose only slightly, from $5.2\times10^{19}$ cm$^{-3}$ at 25 °C to $7.1\times10^{19}$ cm$^{-3}$ at 70 °C (the detailed calculation procedure is described in Eq. (S1)). In contrast, electrochemical impedance spectroscopy (EIS) showed a notable reduction in the impedance arc radius upon heating, which corresponds to a lower charge transfer resistance and more efficient charge transfer at the electrode–electrolyte interface (Fig. 3(d)).[9,10,20,23] Figure S8 presents the significantly increased absorbed photon to current conversion efficiency (APCE) of $\alpha$-$Fe_2O_3$ at elevated temperatures, corresponding to the improved charge collection, as calculated in detail in Eq. (S2).

The most critical factor was identified by analyzing the transfer curves (Figs. 3(e) and 3(f)). From this, the carrier mobility increased dramatically by approximately 6.5 times, from $2.99\times10^{-3}$ cm$^2$/(V·s) at 25 °C to $1.943\times10^{-2}$ cm$^2$/(V·s) at 70 °C, as calculated in Eq. (S3).[33] Therefore, we conclude that the improved PEC performance is primarily driven by the thermally-enhanced carrier mobility. This facilitates the hopping of small polarons within the bulk $\alpha$-$Fe_2O_3$, leading to superior charge separation and transfer efficiency.

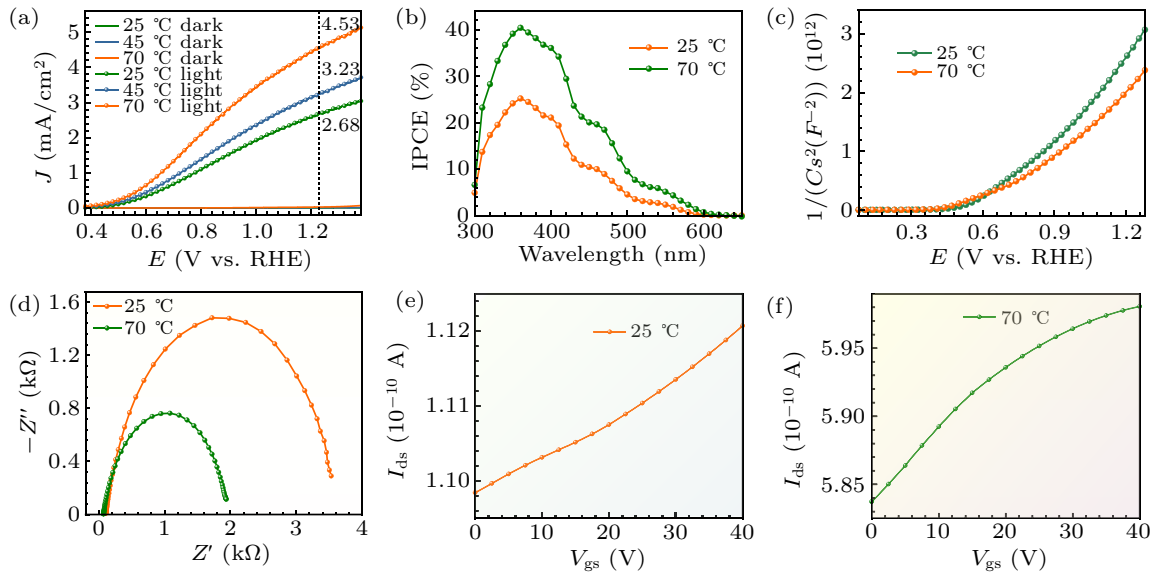



**Fig. 3.** Temperature-regulated PEC performance of $\alpha$-$Fe_2O_3$. (a) LSV curves of $\alpha$-$Fe_2O_3$ annealed in argon at various temperatures; (b) IPCE, (c) MS, and (d) EIS curves of $\alpha$-$Fe_2O_3$ measured at 25 °C and 70 °C. Transfer curves of $\alpha$-$Fe_2O_3$ measured at (e) 25 °C and (f) 70 °C.

Additionally, the $\alpha$-$Fe_2O_3$ film demonstrates promising operational stability. Chronopotentiometry (CP) testing at 70 °C (Fig. S9(a)) reveals an initial gradual increase in current, followed by stabilization and a slight decrease. The transient current spike observed around 32000 s is likely attributable to the detachment of bubbles from the electrode surface. Post-test characterization confirms the structural and chemical integrity of the film. The O 1s XPS spectra (Fig. S9(d)) remain virtually unchanged, showing no indication of excessive oxygen vacancy formation. XRD patterns (Figs. S9(b) and S9(e)) exhibit no peak shifts or new phases, ruling out any phase transformation. Furthermore, SEM images (Figs. S9(c) and S9(f)) confirm that the film remains adherent and intact, with no signs of delamination or morphological degradation. Collectively, these results confirm that the $\alpha$-$Fe_2O_3$ film retains its original morphology, crystal structure, and surface chemistry after 12 h of continuous operation at elevated temperature, underscoring its robust stability.

### 2.3. Thermally-activated carrier dynamics

Elevating the temperature of $\alpha$-$Fe_2O_3$ samples promotes the small polaron hopping, which in turn improves the charge separation and injection efficiency.[10,23] To confirm this, we measured these efficiencies under simulated solar irradiation. Furthermore, the role of small polarons in different hopping modes was tested under 360 nm and 525 nm monochromatic light, corresponding to ligand-to-metal charge transfer (LMCT) and d–d transitions, respectively.[34,35] Calculations of the theoretical maximum photocurrent densities for three wavelengths and the charge separation and injection efficiency are given in Eqs. (S4)–(S6).

Figure 4(a) shows the charge injection ($\eta_{inj}$) and separation ($\eta_{sep}$) efficiencies of $\alpha$-$Fe_2O_3$ under simulated solar light. While heating improves both, the enhancement in $\eta_{sep}$ is more pronounced. These values were calculated by the following equations:

$$\Delta\eta_{inj} = \frac{\eta_{inj}(70\ ^\circ\mathrm{C}) - \eta_{inj}(25\ ^\circ\mathrm{C})}{\eta_{inj}(25\ ^\circ\mathrm{C})} \times 100\%, \quad (1)$$

$$\Delta\eta_{sep} = \frac{\eta_{sep}(70\ ^\circ\mathrm{C}) - \eta_{sep}(25\ ^\circ\mathrm{C})}{\eta_{sep}(25\ ^\circ\mathrm{C})} \times 100\%, \quad (2)$$

$$\alpha_{inj} = \Delta\eta_{inj}/(\Delta\eta_{inj} + \Delta\eta_{sep}) \times 100\%, \quad (3)$$

$$\alpha_{sep} = \Delta\eta_{sep}/(\Delta\eta_{inj} + \Delta\eta_{sep}) \times 100\%, \quad (4)$$

where $\Delta\eta_{inj}$ and $\Delta\eta_{sep}$ represent the percentage increases in charge injection and separation efficiencies, while $\alpha_{inj}$ and $\alpha_{sep}$ represent the percentage increases in charge injection and separation efficiencies as percentages of the total increase. As detailed in Fig. 4(b), which quantifies these percentage increases at different potentials, the photocurrent gain is primarily due to improved charge separation. This confirms that heating's main effect is to facilitate small polaron hopping.

This mechanism is consistent under monochromatic light. Figs. 4(c) and 4(e) present $\eta_{inj}$ and $\eta_{sep}$ under 360 nm and 525 nm light, respectively, with their contributions to photocurrent shown in Figs. 4(d) and 4(f). Under 360 nm light, which excites carriers via LMCT, the absolute $\eta_{sep}$ is higher.[34] LMCT, in Fig. 4(h), involving electron excitation from O 2p to Fe 3d orbitals, directly generates mobile carriers that contribute to photocurrent.[34,36] Under 525 nm light, which induces a d–d transition, the percentage increase in $\eta_{sep}$ upon heating is greater (Fig. 4(g)).[34] The d–d transition is more localized (Fig. 4(i)), creates more small polarons, and does not directly produce mobile carriers.[7,36,37] Consequently, heating has a more significant relative effect by promoting small polaron hopping in this regime.

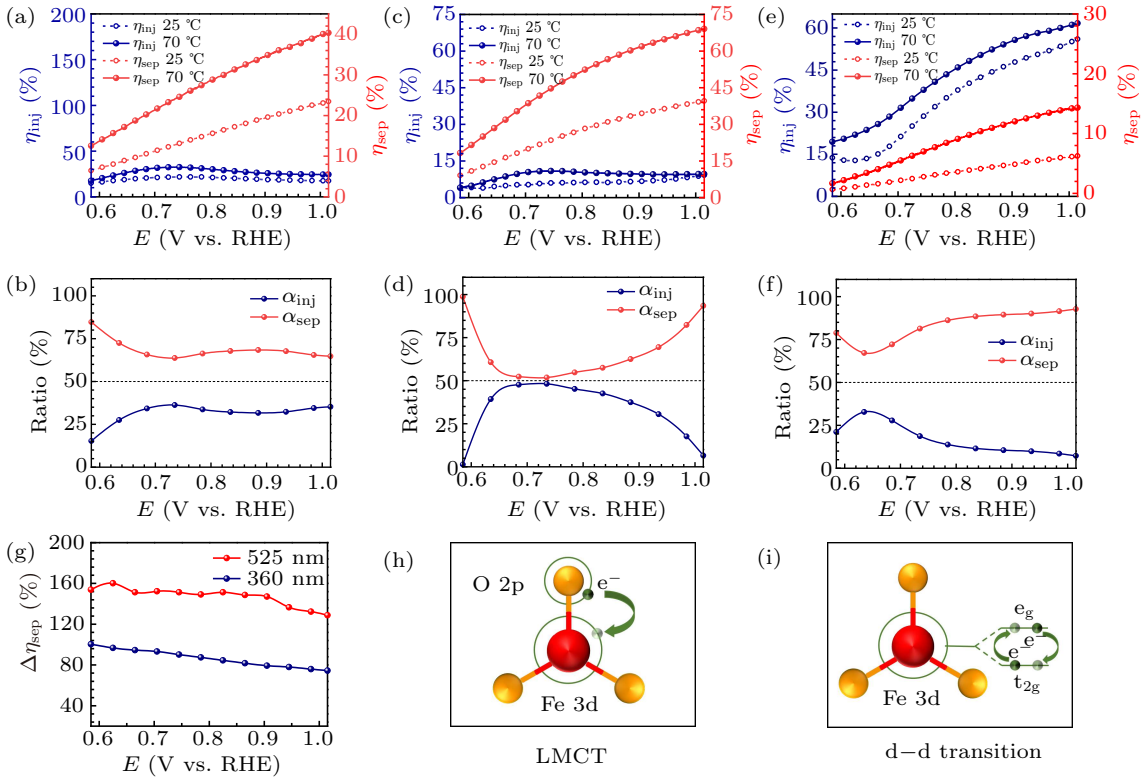



**Fig. 4.** Temperature-regulated carrier dynamics. (a) Injection, separation efficiencies and (b) their corresponding percentage increases of $\alpha$-$Fe_2O_3$ under simulated solar light illumination, (c) and (d) 360 nm monochromatic light illumination, and (e) and (f) 525 nm monochromatic light illumination. (g) Comparison of the percentage increase of separation efficiencies under 525 nm and 360 nm monochromatic light. Schematic of (h) LMCT transition and (i) d–d transition.

To further validate this, we compared $\alpha$-$Fe_2O_3$ samples annealed in argon (creating more $O_V$ and small polarons) with those annealed in air under solar light (Fig. S10). As expected, the argon-annealed samples showed a significantly larger increase in separation efficiency and photocurrent density after heating. This directly demonstrates that enhancing small polaron hopping is crucial for improving PEC performance.

### 2.4. Carrier collection analysis

To evaluate carrier collection and loss during photoelectrode operation intuitively, we employ an optical model based on the transfer matrix method (TMM).[9,38,39] Accurate measurement of the optical constants of thin films is a prerequisite for the construction of the transport matrix model. In this work, a multi-angle elliptical polarimeter combined with parameter fitting was used to extract the optical constants of $\alpha$-$Fe_2O_3$ thin film, and detailed optical constants $n$ and $k$ are provided in Fig. S11. The detailed calculation process is provided in Eqs. (S7)–(S11). Figure 5(a) depicts a schematic of the model's structure, assuming that the $\alpha$-$Fe_2O_3$ photoelectrode anode is one-dimensional and has a completely flat surface. As can be seen, the incident light must pass through numerous layers of media, and phase cancellation is utilized to deal with repeated reflections from incoherent layers. The film's optical constants were eventually employed to calculate the position-dependent photogenerated carrier generation profile within the active layer, as illustrated in Fig. 5(b). The results reveal that the carrier generation rate $G(Z)$ decreases dramatically from surface to film. As previously stated, the regularization procedure generates SLR curve for each IPCE spectrum, which reflects the system's carrier collection characteristics.[7,9,38,39] Figure 5(c) depicts the SLR curve obtained from Fig. 3(b), revealing that the majority of the collected carriers are created within the first 100 nm of the electrode surface. Figure 5(c) shows that the SLR of $\alpha$-$Fe_2O_3$ at 70 °C is much lower than that at

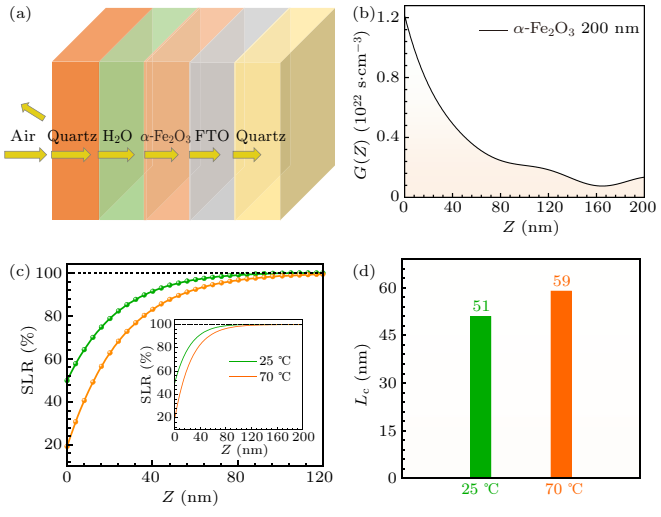



**Fig. 5.** SLR analysis of $\alpha$-$Fe_2O_3$ films. (a) TMM model of the $\alpha$-$Fe_2O_3$ photoelectrode. (b) The photogeneration rate within the $\alpha$-$Fe_2O_3$ film calculated using the TMM. (c) SLR and (d) $L_c$ curves of $\alpha$-$Fe_2O_3$ samples.

25 °C, accounting for approximately 40% of 25 °C at the surface. In the PEC system, the material performance is determined by the minority carrier collection length, $L_c$, which reflects the distance at which the minority carriers effectively affect the surface current.[8,38] By defining $L_c$ as the distance from the position where the carrier collection efficiency is 1/10 of the surface carrier collection efficiency to the surface, Fig. 5(d) shows that the $L_c$ of $\alpha$-$Fe_2O_3$ at 70 °C is 8 nm longer than at 25 °C, implying that increasing the temperature promotes the hopping of the small polarons, resulting in a significant increase in the carrier collection efficiency.[9]

## 3. Conclusions

In summary, we report a thermal activation strategy that dramatically improves the performance of hematite photoanodes by enhancing small polaron hopping, which is the main charge transport mechanism in many transition metal oxides. Unlike conventional doping or passivation, this method uses elevated temperature to directly facilitate polaron hopping, increasing carrier mobility by $\sim 6.5$ times and reducing spatial losses. The thermal effect is most pronounced for charges excited via d–d transitions due to their strong polaronic nature. Consequently, the optimized device achieves a high photocurrent density of 4.53 mA/cm$^2$ at 1.23 V vs. RHE. This work establishes a simple and widely applicable approach to achieve efficient carrier transport in metal oxide photoelectrodes for solar energy conversion.

## Acknowledgements

The authors acknowledge support from the National Key Research and Development Program of China (Grant No. 2022YFC2204101), the National Natural Science Foundation of China (Grant No. 5257022607), the Fundamental Research Funds for the Central Universities (Grant No. lzujbky-2025-ytC02), and the Key Research and Development Program of Gansu Province (Grant No. 24YFGA005). The authors also greatly acknowledge the support of the Supercomputing Center of Lanzhou University, China.

## References

[1] Liu P F, Wang C W, Wang Y, Li Y H, Zhang B, Zheng L R, Jiang Z, Zhao H J and Yang H G 2011 *Sci. Bull.* **66** 1013
[2] Bak A, Choi W and Park H 2011 *App. Catal. B: Environ.* **110** 207
[3] Liu D Y and Kuang Y B 2024 *Adv. Mater.* **36** 2311692
[4] Carneiro L M, Cushing S K, Liu C, Su Y D, Yang P D, Alivisatos A P and Leone S R 2017 *Nat. Mater.* **16** 819
[5] Li C C, Luo Z B, Wang T and Gong J L 2018 *Adv. Mater.* **30** 1707502
[6] Shen S H, Lindley S A, Chen X Y and Zhang J Z 2016 *Energy Environ. Sci.* **9** 2744
[7] Yifat P, David S E, Daniel A G, Anton T and Avner R 2021 *Energy Environ. Sci.* **14** 4584
[8] Hu X Q, Huang J, Cao Y, He B, Cui X, Zhu Y H, Wang Y, Chen Y H, Yang Y K, Li Z and Liu X Q 2023 *Carbon Energy* **5** 369
[9] Shao J L, Wang Y J, Liu H Y, Hao R, Luo L L, Li Y T, Cooper J K and Zhang Z M 2025 *Appl. Phys. Lett.* **126** 223508
[10] Tang S T, Qiu W T, Xu X W, Xiao S, Tong Y X, Wang X W and Yang S H 2022 *Adv. Funct. Mater.* **32** 2110284
[11] Merschjann C, Imlau M, Brüning H, Schoke B and Torbrügge S 2011 *Phys. Rev. B* **84** 052302
[12] Franchini C, Reticcioli M, Setvin M and Diebold U 2021 *Nat. Rev. Mater.* **6** 560
[13] Ren Z Z, Shi Z J, Feng H F, Xu Z F and Hao W C 2023 *Adv. Sci.* **11** 2305139
[14] Cresi J S P, Mario L D, Catone D, Martelli F, Paladini A, Turchini S, D'Addato S, Luches P and O'Keeffe P 2020 *J. Phys. Chem. Lett.* **11** 5686
[15] Rettie A J E, Chemelewski W D, Emin D and Mullins C B 2016 *J. Phys. Chem. Lett.* **7** 471
[16] Wang Z L, Mao X, Chen P, Xiao M, Monny S A, Wang S C, Konarova M, Du A J and Wang L Z 2019 *Angew. Chem. Int. Ed.* **58** 1030
[17] Qiu W T, Xiao S, Ke J W, Wang Z, Tang S T, Zhang K, Qian W, Huang Y C, Huang D, Tong Y X and Yang S H 2019 *Angew. Chem. Int. Ed.* **58** 19087
[18] Li M Y, Yang Y, Ling Y C, Qiu W T, Wang F X, Liu T Y, Song Y, Liu X X, Fang P P, Tong Y X and Li Y 2017 *Nano Lett.* **17** 2490
[19] Xiao Y Q, Fu J, Pihosh Y, Karmakar K, Zhang B B, Domen K and Li Y B 2025 *Chem. Soc. Rev.* **54** 1268
[20] Li X, Hou S S, Xie X X, Yang H and Huang Y C 2026 *J. Catal.* **453** 116540
[21] Zhang L L, Chu W B, Zhao C Y, Zheng Q J, Prezhdo O V and Zhao J 2021 *J. Phys. Chem. Lett.* **12** 2191
[22] Huang J, Hu X Q, Wang J N, Lin K J, He B, Yang Y K, Wang Y, Li Z and Liu X Q 2023 *Chemical Engineering Journal* **462** 142246
[23] Zhang J N, Tang T X, Xie Z Z, Chen Y X, Yang H, Ye K H, Chen J W, Zou W H, Shi J X and Huang Y C 2024 *Chem. Eng. J.* **497** 154833
[24] Machreki M, Chouki T, Martelanc M, Butinar L, Vodopivec B M and Emin S 2021 *J. Environ. Chem. Eng.* **9** 105495
[25] Liu J F, Du S W, Fan W J, Li Q L, Yang Q, Luo L, Li J N and Zhang F X 2024 *Energy Environ. Sci.* **17** 9093
[26] Jin J T, Liu Y C, Zhao X D, Liu H, Deng S Q, Shen Q Y, Hou Y, Qi H, Xing X R, Jiao L F and Chen J 2023 *J. Chen, Angew. Chem. Int. Ed.* **62** 202219230
[27] Li H M, Wang Z Y, Jing H J, Yi S S, Zhang S X, Yue X Z, Zhang Z T, Lu H X and Chen D L 2021 *Applied Catalysis B: Environmental* **284** 119760
[28] Li H L, Guo M, Zhou Z H, Long R and Fang W H 2023 *J. Phys. Chem. Lett.* **14** 2448
[29] Hu Z J, Bao Y J, Li Z W, Gong Y J, Feng R, Xiao Y D, Wu X C, Zhang Z H, Zhu X, Ajayan P M and Fang Z Y 2017 *Sci. Bull.* **62** 16
[30] Gong X N, Wu H, Yang D F, Zhang B, Peng K L, Zou H J, Guo L J, Lu X, Chai Y S, Wang G Y and Zhou X Y 2020 *Vib. Spectrosc.* **107** 103034
[31] Jang A R, Yoon J W, Son S B, Ryu H I, Cho J, Shin K H, Sohn J I and Hong W K 2021 *ACS Appl. Mater. Interfaces* **13** 3426
[32] Bergeron A, Gradziel C, Leonelli R and Francoeur S 2023 *Nat. Commun.* **14** 4098
[33] Wang N, Mao N N, Wang Z E, Yang X, Zhou X, Liu H N, Qiao S L, Lei X F, Wang J R, Xu H, Ling X, Zhang Q Y, Feng Q L and Kong J 2021 *Adv. Mater.* **33** 2005815
[34] Hayes D, Hadt R G, Emery J D, Cordones A A, Martinson A B F, Shelby M L, Fransted K A, Dahlberg P D, Hong J Y, Zhang X Y, Kong Q Y, Schoenlein R W and Chen L X 2016 *Energy Environ. Sci.* **9** 3754
[35] Kay A, Fiegenbaum-Raz M, Müller S, Eichberger R, Dotan H, Krol R V D, Abdi F F, Rothschild A, Friedrich D and Grave D A 2020 *Adv. Funct. Mater.* **30** 1901590
[36] Grave D A and Segev G 2022 *J. Phys. D: Appl. Phys.* **55** 023001
[37] Grave D A, Ellis D S, Piekner Y, Kölbach M, Dotan H, Kay A, Schnell P, Krol R V D, Abdi F F, Friedrich D and Rothschild A 2021 *Nat. Mater.* **20** 833
[38] Segev G, Jiang C M, Cooper J K, Eichhorn J, Toma F M and Sharp I D 2018 *Energy Environ. Sci.* **11** 904
[39] Segev G, Dotan H, Ellis D S, Piekner Y, Klotz D, Beeman J W, Cooper J K, Grave D A, Sharp I D and Rothschild A 2018 *Joule* **2** 1